Appl. Phys. B 69, 257–261 (1999) / Digital Object Identifier (DOI) 10.1007/s003409900123

Applied Physics B
Lasers
and Optics

Three-body decay of a rubidium Bose–Einstein condensate

J. Söding, D. Guéry-Odelin, P. Desbiolles, F. Chevy, H. Inamori, J. Dalibard

Laboratoire Kastler Brossel*, Ecole Normale Supérieure, 24 rue Lhomond, F-75231 Paris CEDEX 05, France

Received: 24 November 1998/Revised version: 26 June 1999/Published online: 8 September 1999

Abstract. We have measured the three-body decay of a Bose–Einstein condensate of rubidium (^{87}Rb) atoms prepared in the doubly polarized ground state $F = m_F = 2$. Our data are taken for a peak atomic density in the condensate varying between $2 \times 10^{14}\,\mathrm{cm}^{-3}$ at initial time and $7 \times 10^{13}\,\mathrm{cm}^{-3}$, 16 s later. Taking into account the influence of the uncondensed atoms on the decay of the condensate, we deduce a rate constant for condensed atoms $L = 1.8\,(\pm 0.5) \times 10^{-29}\,\mathrm{cm}^6\,\mathrm{s}^{-1}$. For these densities we did not find a significant contribution of two-body processes such as spin dipole relaxation.

PACS: 03.75.Fi; 34.50.Pi; 32.80.Pj

The remarkable achievement of Bose–Einstein condensation in alkali vapors opens the way to many spectacular applications of ultra-cold atomic gases [1–3]. For most if not all of these applications, it is important to estimate the stability of the condensate with respect to inelastic processes, since the condensate lifetime ultimately determines the available time for a given experiment.

Two kinds of inelastic processes can contribute significantly to the decay of a Bose–Einstein condensate: three-body recombination and two-body spin relaxation. In the first process, when three atoms are close to each other, two of them may form a dimer or molecule, generally in an excited vibrational state, and the third atom carries away the released energy. Since this energy is much larger than the typical depth of the trap confining the atoms, the three atoms are lost. For an atom in $\mathbf{r}$, the probability per unit time for this process is proportional to $n^2(\mathbf{r})$, where $n(\mathbf{r})$ is the spatial density of the atomic sample. The second process can occur if the atoms are confined in a magnetic trap. In this case the atoms are prepared in a low-field seeking state, which is not the lowest atomic state. The magnetic dipole interaction during a collision between two trapped atoms can lead to a spin flip which releases the Zeeman energy $\Delta E \propto \mu_\mathrm{B} B$, where μ_B is the Bohr magneton and B the local magnetic field. For this second process, the probability per unit time that an atom in $\mathbf{r}$ is expelled from the trap is proportional to $n(\mathbf{r})$.

In this paper we present experimental results concerning the decay of a ^{87}Rb condensate prepared in the doubly polarized ground state $F = m_F = 2$ and confined in a magnetic trap. We monitor the time evolution of the number of atoms in the condensate for 16 s, the condensed fraction remaining always higher than 40%. We show that for our average densities in the condensate (between $4 \times 10^{13}\,\mathrm{cm}^{-3}$ and $12 \times 10^{13}\,\mathrm{cm}^{-3}$), the three-body recombination is the dominant loss process and we determine the corresponding rate coefficient. By contrast, we do not find evidence for two-body spin relaxation.

1 Experimental

Our experimental setup is based on two glass cells, one positioned 70 cm above the other. Each is evacuated by a 25-l/s ion pump, and they are connected through a narrow glass tube (∅ 9 mm, length 140 mm) to allow differential pumping. The lower cell is also connected to a titanium sublimation pump. This system allows us to produce a good vacuum in the lower cell (lifetime of the magnetic trap ≈ 40 s) while having sufficient Rb vapor pressure in the upper cell to load a magneto-optical trap (MOT) in ≈ 0.3 s.

Light in the experiment is provided wholly by diode lasers at the rubidium resonance (780 nm). The experimental sequence begins by loading 3×10^7 atoms into the upper MOT in 190 ms. These atoms are then pushed towards the lower cell by a 10-ms pulse from a vertical resonant laser beam. The measured final atomic velocity is 14 m/s. The atoms are then recaptured in the lower MOT. The transfer efficiency is 70%, measured using a time-of-flight method based on the absorption of a probe beam located 2 cm below the center of the trap. We repeat this loading sequence 50 times while the lower MOT is operating. After 10 s, 10^9 atoms are captured in the lower MOT[1]. The atoms are then cooled by a 10-ms molasses phase and transferred into the magnetic trap.

* Unité de recherche de l'ENS et de l'Université Pierre et Marie Curie, associée au CNRS

[1] By increasing the number of loading sequences to 100, we could load up to 1.6×10^9 atoms, but this was not necessary for the experiments described here.

This trap is of the Ioffe–Pritchard type, i.e. it is purely static and it consists of a nonzero local magnetic field minimum. The field is generated by three identical circular coils whose axes point towards $+x$, $-x$, $+y$ respectively (z denotes the vertical axis), and whose centers are at equal distance from the center O of the trap. The same current runs through the three coils. These coils have a conical shape so that 4 of the 6 lower MOT beams can be placed with a $\approx 45°$ angle with respect to the horizontal plane (Fig. 1). Each coil has 80 turns, is water cooled, and can be run with a current of 100 A. For the experiments described below, a current of 46 A only was used. The leading terms in the magnetic field variations around O are $(b'x, B_0 + b''(2y^2 - x^2 - z^2)/4, -b'z)$, with $B_0 = 12.9\,\mathrm{mT}$, $b' = 1.39\,\mathrm{T\,m^{-1}}$, $b'' = 84.5\,\mathrm{T\,m^{-2}}$, for a 46 A current. These quantities are accurately determined from the oscillation frequencies of the center of mass of the trapped atomic cloud.

At the end of the molasses phase, the atoms are optically pumped into the doubly polarized state $F = m_F = 2$ (quantization axis y), and the magnetic trap is switched on. The transfer efficiency from the MOT to the magnetic trap is 50%. The atomic cloud is then further compressed by reducing the bias field B_0 to 0.126 mT using a pair of Helmholtz coils aligned with the y axis. The transverse oscillation frequency $\omega_{x,z} \simeq (\mu_B b'^2/m B_0)^{1/2}$ increases to $2\pi \times 157$ Hz, while the longitudinal frequency $\omega_y = (\mu_B b''/m)^{1/2}$ remains equal to $2\pi \times 11.7$ Hz (m is the atomic mass). At the end of this compression stage, the temperature is 200 μK.

We then perform forced evaporative cooling using a sweeped radio-frequency field ν_{RF}. The function $\nu_{RF}(t)$ is optimized so as to maximize the number of condensate atoms after an 18-s duration. The optimum shape is found to be very close to an exponential law $\nu_a + \nu_b\, e^{-t/\tau}$ with a time constant $\tau = 3.5$ s. The initial value for ν_{RF} is 15 MHz and the final one is 0.900 MHz. This final value is 10 kHz above the value $\nu_{min} = 0.890$ MHz which empties completely the trap. At this stage a condensate is formed.

The frequency ν_{RF} is subsequently kept constant for 2 s at 0.900 MHz to ensure that thermal equilibrium is reached and is then ramped up to 0.910 MHz in 0.1 s. This corresponds to the initial time of the relaxation experiment. The atoms evolve now in the magnetic trap for an adjustable time t between 0 and 16 s, with the rf on at the fixed value 0.910 MHz. This rf shield limits the trap depth to ≈ 0.8 μK, in order to ensure that any atom which has been heated after an inelastic event leaves the trap quasi-immediately.

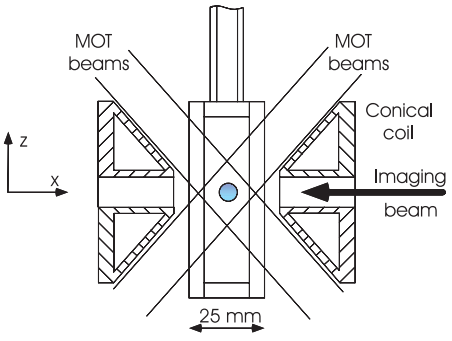

Fig. 1. Cut through the lower glass cell and two of the three conical magnetic field coils generating the trapping potential. The third pair of MOT beams is perpendicular to the plane of the figure

The detection of the atomic cloud remaining in the trap after a relaxation time t is made using an absorption imaging technique. The magnetic trap is switched off in 300 μs, and the atoms fall freely during 32 ms. A 35-μs pulse from a weak ($55\,\mu\mathrm{W\,cm^{-2}}$) linearly polarized probe beam propagating along the x axis then illuminates the atomic cloud. An optical system with a 1.64 magnification images the probe beam with the atomic cloud onto a CCD array. A second image with no atoms is taken 200 ms later to determine the laser intensity profile. The logarithm of the ratio of the two images yields the cloud's optical density $d(y,z) = \sigma \int n_{tot}(\mathbf{r})\, \mathrm{d}x$, where σ is the absorption cross-section and $n_{tot}(\mathbf{r}) = n(\mathbf{r}) + n_{th}(\mathbf{r})$ the total (condensed + thermal) spatial density of the sample.

We choose a beam resonant with the atomic transition $5s_{1/2} \rightarrow 5p_{3/2}$. To stay within the limits of the camera sensitivity, we make sure that the optical density remains below 3 (95% absorption). This limitation to relatively dilute samples could be circumvented by taking an image with a laser beam detuned from the atomic resonance. However, we found that the dispersive nature of the cloud for a nonzero detuning makes the accurate calibration of the size of the images more delicate.

The experimental value for the resonant cross-section is adjusted so that the measured critical temperature is equal to the predicted one [4]. We obtain $\sigma = 0.36\,\sigma_0$, where $\sigma_0 = 3\lambda^2/(2\pi)$ is the resonant cross-section for an atomic transition with a Clebsh–Gordan coefficient equal to 1. For unpolarized atoms, the expected value would be $0.47\,\sigma_0$, obtained from the average of the squares of the corresponding Clebsh–Gordan coefficients. The ab initio determination of σ would require the knowledge of the exact polarization state of the atoms after the time of flight, as well as the contribution of the linewidth (≈ 1 MHz) of the probe laser.

2 Results and discussion

A typical image consists of two features: (i) a central elliptic region of high density corresponds to the condensate cloud. At $t = 0$, the total size of this region is $\Delta y \times \Delta z = 130\,\mu\mathrm{m} \times 270\,\mu\mathrm{m}$. (ii) a slightly larger quasi-isotropic region corresponds to the uncondensed fraction of the atomic cloud. The analysis of the images is made by a 2-step fitting procedure. In a first step, we fit only the part of the image that contains no condensate by a Gaussian function to derive the temperature T. In a second step, we substract the Gaussian distribution derived in this way and we fit only the central component to derive precisely the number of condensed atoms N. This second fit is performed using a function corresponding to the integration along the x axis of a paraboloidal distribution. The latter describes in the Thomas–Fermi limit [5] the equilibrium density profile of the condensate within the harmonic trap, and it is known to remain valid (with a scaling factor) after a ballistic expansion [6]. The total number of atoms N_{tot} is finally evaluated from the integral of $d(y,z)$ over the whole image[2].

[2] We have also developed a more sophisticated procedure for the determination of the temperature assuming an ideal Bose–Einstein distribution for the uncondensed fraction rather than a Maxwell–Boltzmann distribution. Since an accurate determination of the temperature (i.e. to better than 10%)

To accurately measure the decrease of the number N of atoms in the condensate, drifts and fluctuations in the initial number of condensed atoms and in the temperature have to be suppressed as far as possible. The most important limitation to experimental accuracy is the drift of the magnetic field minimum B_0. A decrease of B_0 by only 10^{-6} T will diminish $\nu_{\min}$ by 7 kHz. Because the cold atomic samples are prepared by evaporating down to a *fixed* final rf frequency with $U_0/k_{\rm B}T \approx 5$ (U_0: trap depth), this decrease corresponds to a temperature increase of $\approx (h/k_{\rm B})\,(7/5)\text{kHz} = 70$ nK. This value has to be compared to our typical transition temperature $T_{\rm c} \approx 200$ nK. In order to keep the initial fraction of condensed atoms stable around 75%, the magnetic field minimum B_0 has to be stable to within 10^{-6} T. This is a very stringent condition because the value $B_0 \approx 10^{-4}$ T is obtained by subtracting two large ($\approx 10^{-2}$ T) nearly equal fields.

In normal operation we have observed drifts in the value of B_0 on the order of 10^{-5} T. We have identified temperature changes of the magnetic field coils and their support structure as primary source for these drifts. Temperature changes lead to thermal dilations by a few μm that can account for the observed drifts. To get rid of these drifts we have automatized the experiment and data acquisition completely. This allows us to leave the laboratory while the computer is producing one condensate every ≈ 35 s, varying the relaxation time of the cloud in the magnetic trap automatically. After 15 min the setup is in thermal equilibrium and drifts of B_0 are below 3×10^{-7} T during one data series (≈ 1.5 h).

To reduce systematic errors due to residual drifts in B_0 even further, we have put a set of 16 different relaxation times t in random order and repeated this same set 9 times in a row, thus preparing 16×9 condensates in total. For each relaxation time we measure the number of atoms remaining in the condensate. Finally, we calculate their average $\bar{N}(t) = (1/9) \sum N_i(t)$.

The number $\bar{N}(t)$ of condensate atoms is shown in Fig. 2 on a logarithmic scale. The marked non-exponential decay indicates that in the beginning the atoms are lost mainly by two- or three-body inelastic collisions. The initial and final numbers of atoms in the condensate are respectively 300 000 and 17 000, and the initial and final average condensate densities are $11.8 \times 10^{13}\,\text{cm}^{-3}$ and $3.8 \times 10^{13}\,\text{cm}^{-3}$. The temperature of the sample is constant at 75 ($\pm$13) nK over the measured time interval.

We now compare the measured atom number in the condensate with the solution of the differential equation governing the time evolution of N. In a first step we consider only collisions between condensate atoms. The loss rates due to two- and three-body collisions are described by terms $-G \int n^2(\mathbf{r})\ \mathrm{d}^3r = -G\langle n\rangle N$ and $-L \int n^3(\mathbf{r})\ \mathrm{d}^3r = -L\langle n^2\rangle N$, respectively, where G and L are the rate coefficients for two- and three-body collisions, and where we put for a function $\eta(\mathbf{r})$: $\langle\eta\rangle = \int \eta(\mathbf{r})\, n(\mathbf{r})\ \mathrm{d}^3r\ /\ N$. The integrals can be calculated in the Thomas–Fermi limit of a parabolic condensate density, giving $\langle n\rangle = c_2 N^{2/5}$ and $\langle n^2\rangle = c_3 N^{4/5}$, with $c_2 = (15^{2/5}/(14\pi))\left(m\bar{\omega}/(\hbar\sqrt{a})\right)^{6/5}$ and $c_3 = (7/6)c_2^2$. Here $a = 5.8$ nm denotes the scattering length and $\bar{\omega} = (\omega_x\omega_y\omega_z)^{1/3}$. The validity of the Thomas–Fermi approximation can be checked in Fig. 3, where we have plotted

is not essential for the present work, we have used here only the simpler fitting procedure.

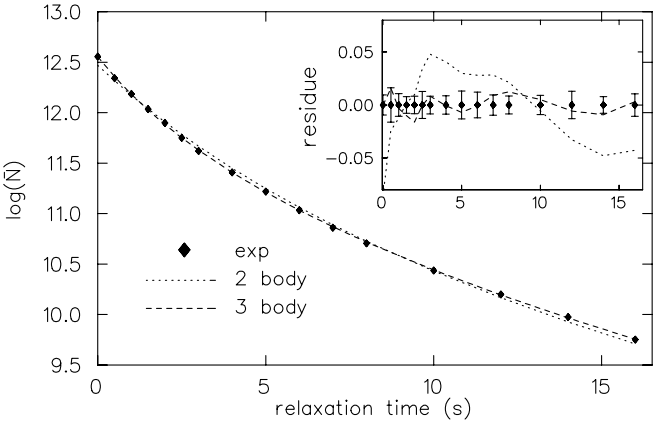

Fig. 2. Logarithm of total number of atoms remaining in the condensate after a relaxation time t. Each point is an average over 9 measurements. The *inset* shows the deviation of the experimental points from a fit to a two-body decay law (*dotted line*) and to a three-body decay law (*dashed line*). The *error bars* indicate the statistical error for each point

the full width Δz of the condensate as a function of N, together with a fit using the modelling function $\Delta z = \Delta z_1\, N^{1/5}$. We find $\Delta z_1 = 21.2\,\mu$m, in very good agreement (to within 4%) with the Thomas–Fermi prediction $\Delta z_1 = 20.4\,\mu$m [6].

We have not been able to find an analytical solution to the differential equation describing both two- *and* three-body collisions at the same time, but we can solve the equation in the presence of either two- or three-body collisions:

$$\frac{1}{N}\frac{\mathrm{d}N}{\mathrm{d}t} = -Gc_2N^{2/5} - \frac{1}{\tau}\,, \tag{1}$$

$$\frac{1}{N}\frac{\mathrm{d}N}{\mathrm{d}t} = -Lc_3N^{4/5} - \frac{1}{\tau}\,. \tag{2}$$

The dotted and dashed lines in Fig. 2 show solutions of the differential equations for two- and three-body collisions that fit the experimental data best. We find $\{\tau = \infty\,,\ G = 2.78\,(\pm 0.02) \times 10^{-15}\,\text{cm}^3\,\text{s}^{-1}\}$ for two-body collisions and $\{\tau = 14.8\,\text{s}\,,\ L = 2.23\,(\pm 0.11) \times 10^{-29}\,\text{cm}^6\,\text{s}^{-1}\}$ for three-body collisions, where the error is purely statistical at this

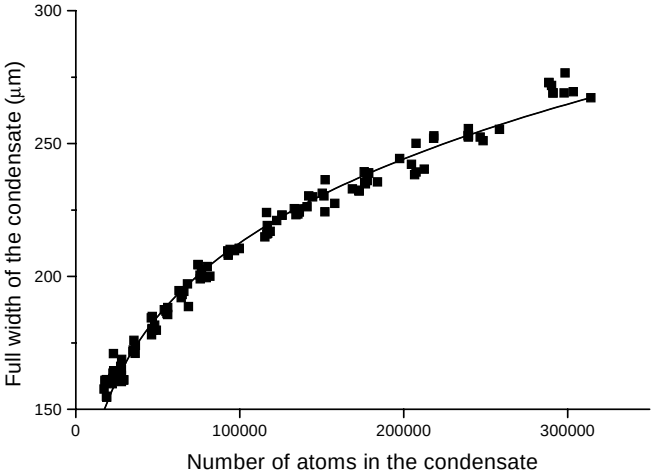

Fig. 3. Variations of the full width Δz of the condensate along the z axis, as a function of the number of condensed atoms N. The *full line* is a fit with the function $\Delta z = \Delta z_1\, N^{1/5}$

stage. The lifetime of the condensate τ is determined by small-angle collisions with the thermal background gas and expected to be smaller than the lifetime of an uncondensed cloud. Indeed a small energy on the order of 100 nK (the chemical potential) is sufficient to eject the atoms out of the condensate, whereas an energy of ≈ 1 mK is necessary to make an atom leave the magnetic trap. We found a lifetime for thermal clouds $\tau_{\rm th} \approx 40$ s, which contradicts the two-body hypothesis.

The error bars in the inset show the statistical error for $\bar{N}$. The noise on the number of atoms can be read directly from the length of the error bars and it amounts to only 1%. The difference between the experimental data and the best fit is shown with dashed and dotted lines. Whereas the residue of the fit to a three-body decay law (dashed line) stays most of the time within the bounds given by the statistical error, the fit to a two-body decay law has deviations by several σ for many points. On the basis of our model, a pure two-body decay (including $-1/\tau$) can therefore be ruled out with certainty, whereas a pure three-body decay is well compatible with the data.

More quantitatively, the expected mean value of a χ^2 distribution with 13 degrees of freedom (16 data points minus 3 fit parameters) is 13. The χ^2 value for the two-body fit is $\chi^2 = 235$, corresponding to a rejection confidence much below 10^{-2}, whereas the χ^2 value for three-body decay of $\chi^2 = 12.7$ corresponds to what is to be expected statistically.

Our analysis so far relies on solving the differential equation for $N(t)$, which implies two drawbacks. (i) It neglects collisions of condensate atoms with the thermal component of the cloud. This is not a very good approximation, because the central density of the thermal cloud $n_{\rm th}(\mathbf{r} = \mathbf{0})$ reaches 17% of the mean condensate density $\langle n \rangle$ in the measured time interval. (ii) We can not take account of both two-body and three-body collisions at the same time, making it impossible to place a stringent upper limit on the two-body rate coefficient G.

In presence of collisions with the thermal cloud with density $n_{\rm th}(\mathbf{r})$ the differential equation for $N(t)$ has to be modified:

$$\frac{1}{N}\frac{\mathrm{d}N}{\mathrm{d}t} = -L\left[\langle n^2\rangle + 6\langle n\, n_{\rm th}\rangle + 6\langle n_{\rm th}^2\rangle\right] - G\left[\langle n\rangle + 2\langle n_{\rm th}\rangle\right] - \frac{1}{\tau}\,. \tag{3}$$

The first term on the right-hand side represents three-body collisions, with three, two, or one condensate atom participating in the collision (and being subsequently lost). Similarly, the second term on the right-hand side represents two-body collisions with two or one condensate atoms participating. In writing this equation we have taken into account the role of the symmetry of the condensate wave function with respect to particle exchange [7, 9].

In view of the good quality of the data we now calculate the time derivative of $\ln N$ (equal to $\mathrm{d}N/N\,\mathrm{d}t$) and its statistical error directly from the experimental data[3]. The result is plotted in Fig. 4 as a function of $f(N, T)$, the term multiplying L in (3):

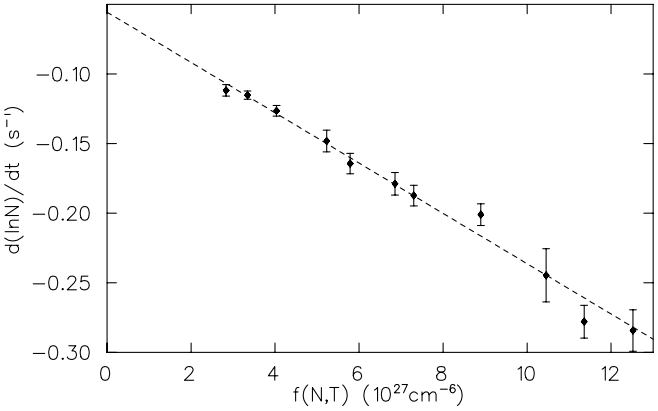

Fig. 4. Logarithmic derivative of the measured number of condensate atoms as a function of $f(N, T)$ (see (4)). The function f is chosen to give a linear dependence for a three-body decay even in the presence of a nonnegligiable thermal background. The *dashed line* shows this linear fit

$$f(N, T) = \langle n^2\rangle + 6\langle n\, n_{\rm th}\rangle + 6\langle n_{\rm th}^2\rangle\,, \tag{4}$$

which is evaluated in the appendix. Points to the right correspond to large atom numbers and short relaxation times. If two-body collisions are negligible, (3) tells us that $\mathrm{d}N/N\,\mathrm{d}t$ depends linearly on $f(N, T)$. Figure 4 reveals exactly this linear dependence, the fit yielding $\tau = 18.0\ (\pm 1.0)$ s and

$$L = 1.80(\pm 0.06 \pm 0.40) \times 10^{-29}\ \mathrm{cm^6\,s^{-1}}\,. \tag{5}$$

The first error represents the *statistical* error, whereas the second, dominating error gives the *systematic* error of 20% due essentially to the calibration of the number of atoms detected. We have found that a nonzero value for the two-body rate G degrades the quality of the fit. For instance taking $G = 10^{-15}\ \mathrm{cm^3 s^{-1}}$, which is a typical expected value for such a process [8], we get a χ^2/degree of freedom equal to 1.26 (confidence level 23%, $L = 1.25 \times 10^{-29}\ \mathrm{cm^6\,s^{-1}}$) instead of 0.91 (confidence level 54%) for the fit with $G = 0$.

In the previous analysis we have assumed that for each three-body collision, only the three atoms that are directly involved in the collision are lost from the trap. In fact, secondary collisions between condensate atoms and fast atoms emerging from a three-body collison might augment the loss of condensate atoms per three-body collision to a value larger than three. We calculate the mean free path of a fast atom by estimating the collisional cross section from a semiclassical model, and obtain $\sigma < 10^{-12}\ \mathrm{cm^2}$ for a relative velocity larger than $10\ \mathrm{ms^{-1}}$. The mean free path ($> 80\ \mu$m) is then larger than the transverse size of the condensate (8 μm full width), so that this effect only plays a minor role.

We now briefly compare our results with previous measurements and predictions. The three-body recombination rate has been measured for Rb atoms prepared in the low hyperfine state $F = -m_F = 1$ [9]. The result for that state is $L = 5.8 \times 10^{-30}\ \mathrm{cm^6\,s^{-1}}$ for condensed atoms, i.e. 3 times smaller than the result found here for the stretched state $F = m_F = 2$. Two theoretical predictions have been made for the three-body recombination rate of Rb, based on different assumptions. A first calculation, based on the Jastrow approximation, led to a very small value $L = 0.7 \times 10^{-30}\ \mathrm{cm^6\,s^{-1}}$

[3] For every set of three adjacent times t_{i-1}, t_i, t_{i+1} we find the parabola that passes through the three data points $\ln \bar{N}_{i-1}$, $\ln \bar{N}_i$, $\ln \bar{N}_{i+1}$ and take the slope of the parabola at time t_i as the value of $\mathrm{d}\ln N/\mathrm{d}t$ at time t_i.

for condensed atoms [10]. A second prediction considers the case of a large and positive scattering length a for the binary elastic collision, corresponding to the existence of a weakly bound state [11]. The recombination rate to this bound state is then shown to be[4] $L = 3.9\hbar a^4/(2m) = 1.6 \times 10^{-30}\,\mathrm{cm}^6\,\mathrm{s}^{-1}$, with $a = 5.8$ nm. Note that the hypothesis at the basis of [11] is not strictly valid for Rb atoms. Clearly more theoretical work is needed to give a quantitative account of the measured rate, for both hyperfine states. Concerning the two-body spin relaxation it has been pointed out [8] that it should be anomalously small ($1\text{–}2 \times 10^{-15}\,\mathrm{cm}^3\,\mathrm{s}^{-1}$ for a field of 10^{-4} T) due to the coincidence of the scattering lengths for elastic collisions in the states $F = m_F = 2$ and $F = -m_F = 1$; our result is in agreement this prediction.

3 Conclusion

We have presented measurements of the inelastic collision rate of a magnetically trapped Bose–Einstein condensate of Rb atoms in their upper hyperfine state. Our analysis, which includes the influence of the thermal component of the atomic cloud, allows us to determine the value of the rate coefficient of three-body collisions. We have discussed possible limitations of our analysis by additional loss mechanisms and find them to be negligible.

Note added in proof

A recent theoretical work [12] gives the 3-body recombination rate in a spin polarized gas as a function of the 2-body scattering length. For the case of ^{87}Rb, this prediction is in excellent agreement with our experimental result.

Acknowledgements. J. S. acknowledges support by the Alexander von Humboldt foundation. This work was partially supported by CNRS, Collège de France, DRET, DRED, and EC (TMR network ERB FMRX-CT96-0002).

Appendix A. Decay rate from a condensate in presence of a thermal component

The decay rate of the condensate via a p-body collision may involve either a collision between p condensate atoms, or a collision between q ($< p$) condensate atoms and $p-q$ atoms from the thermal fraction. Taking into account symmetrization [7], this decay rate can be written:

$$\dot{N} = -\,G \left(\int n^2(\mathbf{r})\ \mathrm{d}^3 r + 2 \int n(\mathbf{r})\, n_{\mathrm{th}}(\mathbf{r})\ \mathrm{d}^3 r \right) \qquad \text{(A.1)}$$

for a two-body process and

$$\dot{N} = -\,L \left(\int n^3(\mathbf{r})\ \mathrm{d}^3 r + 6 \int n^2(\mathbf{r})\, n_{\mathrm{th}}(\mathbf{r})\ \mathrm{d}^3 r + 6 \int n(\mathbf{r})\, n_{\mathrm{th}}^2(\mathbf{r})\ \mathrm{d}^3 r \right) \qquad \text{(A.2)}$$

[4] We deduce this number from [11] by taking into account the reduction by a factor 6 for condensate atoms, and the fact that the three atoms are lossed in an 3-body recombination event.

for a three-body process. As indicated in the text we calculate the first integral of each of these two expressions in the Thomas–Fermi limit, assuming a parabolic condensate density

$$n(\mathbf{r}) = (\mu - V(\mathbf{r}))/g$$

inside the condensate, and $n(\mathbf{r}) = 0$ outside. Here μ is the chemical potential, $V(\mathbf{r})$ denotes the harmonic trapping potential and $g = 4\pi\hbar^2 a/m$.

To evaluate $n_{\mathrm{th}}(\mathbf{r})$ in the remaining terms, we use the Hartree–Fock approximation [5]. Since the density of the thermal fraction is always smaller than the central density of the condensate by an order of magnitude, we neglect the effect of the thermal component on the condensate distribution. In this approximation the density of the thermal fraction is given by:

$$n_{\mathrm{th}}(\mathbf{r}) = \Lambda_T^{-3}\, g_{3/2}\left(e^{-|\mu - V(\mathbf{r})|/k_{\mathrm{B}}T}\right)$$

where $\Lambda_T = h/\sqrt{2\pi m k_{\mathrm{B}} T}$ and $g_{3/2}(z) = \sum z^\ell \ell^{-3/2}$. This expression takes into account the repulsion of the uncondensed atoms from the condensate by the interaction potential $2gn(\mathbf{r})$. The overlap integrals entering in (A.1) and (A.2) are then calculated numerically.

The final results can be cast in the form:

$$\frac{\dot{N}}{N} = -\,L\left(\langle n^2\rangle + 6\,\langle n\rangle\,\tilde{n}_{\mathrm{th}}(\mathbf{0})\,\alpha(\tilde{\mu}) + 6\,\tilde{n}_{\mathrm{th}}^2(\mathbf{0})\,\beta(\tilde{\mu})\right) - G\left(\langle n\rangle + 2\,\tilde{n}_{\mathrm{th}}(\mathbf{0})\gamma(\tilde{\mu})\right),$$

with $\tilde{\mu} = \mu/(k_{\mathrm{B}}T)$. The quantity $\tilde{n}_{\mathrm{th}}(\mathbf{0}) = \Lambda_T^{-3} g_{3/2}(1)$ represents the uncondensed density of an ideal Bose gas at temperature T (below T_{c}) at the center of the trap. The functions α, β, γ are equal to 1 in the limit $\mu \ll k_{\mathrm{B}}T$ and smaller than 1 otherwise, since the overlap between $n(\mathbf{r})$ and $n_{\mathrm{th}}(\mathbf{r})$ is then reduced. For instance, for $\mu = k_{\mathrm{B}}T$ (experimental situation at $t = 0$), we find $\alpha(1) = 0.26$, $\beta(1) = 0.11$, and $\gamma(1) = 0.31$. The effect of mixed collisions (condensate + thermal fraction) is therefore notably reduced with respect to the ideal gas case.

References

1. M.H. Anderson, J.R. Ensher, M.R. Matthews, C.E. Wieman, E.A. Cornell: Science **269**, 1989 (1995)
2. C.C. Bradley, C.A. Sackett, R.G. Hulet: Phys. Rev. Lett. **78**, 985 (1997); see also C.C. Bradley, C.A. Sackett, J.J. Tollet, R.G. Hulet: Phys. Rev. Lett. **75**, 1687 (1995)
3. K.B. Davis, M.-O. Mewes, M.R. Andrews, N.J. van Druten, D.S. Durfee, D.M. Kurn, W. Ketterle: Phys. Rev. Lett. **75**, 3969 (1995)
4. S. Giorgini, L. Pitaevskii, S. Stringari: Phys. Rev. A **54**, 4633 (1996)
5. See for example F. Dalfovo, S. Giorgini, L. Pitaevskii, S. Stringari: to appear in Rev. Mod. Phys.
6. Y. Castin, R. Dum: Phys. Rev. Lett. **77**, 5315 (1996)
7. Y. Kagan, B.V. Svistunov, G.V. Shlyapnikov: JETP Lett. **42**, 209 (1985)
8. P.S. Julienne, F.H. Mies, E. Tiesinga, C.J. Williams: Phys. Rev. Lett. **78**, 1880 (1997)
9. E.A. Burt, R.W. Ghrist, C.J. Myatt, M.J. Holland, E.A. Cornell, C.E. Wieman: Phys. Rev. Lett. **79**, 337 (1997)
10. A.J. Moerdijk, H. Boesten, B.J. Verhaar: Phys. Rev. A **53**, 916 (1996)
11. P.O. Fedichev, M.W. Reynolds, G.V. Shlyapnikov: Phys. Rev. Lett. **77**, 2921 (1996)
12. B.D. Esry, C.H. Greene, J.P. Burke: Phys. Rev. Lett. **83**, 1751 (1999)